Semiconductor Science and Technology

PAPER • OPEN ACCESS

Impact of CdSeTe and CdSe film deposition parameter on the properties of CdSeTe/CdTe absorber structure for solar cell applications

To cite this article: Ali Çiriş *et al* 2024 *Semicond. Sci. Technol.* **39** 025012

OPEN ACCESS
IOP Publishing
Semiconductor Science and Technology
Semicond. Sci. Technol. **39** (2024) 025012 (12pp)
https://doi.org/10.1088/1361-6641/ad1c4d

Impact of CdSeTe and CdSe film deposition parameter on the properties of CdSeTe/CdTe absorber structure for solar cell applications

Ali Çiriş[1,*], Yavuz Atasoy[1,2], Murat Tomakin[3], Abdullah Karaca[4,5], Tayfur Küçükömeroğlu[5] and Emin Bacaksız[5]

[1] Niğde Ömer Halisdemir University, Nanotechnology Application and Research Center, Niğde, Turkey
[2] Niğde Ömer Halisdemir University, Niğde Zübeyde Hanım Vocational School of Health Services, Niğde, Turkey
[3] Department of Physics, Recep Tayyip Erdoğan University, Rize, Turkey
[4] Department of Physics, Yozgat Bozok University, Yozgat, Turkey
[5] Department of Physics, Karadeniz Technical University, Trabzon, Turkey

E-mail: aliciris@ohu.edu.tr

Received 31 July 2023, revised 20 December 2023
Accepted for publication 8 January 2024
Published 23 January 2024

Abstract

In this study, the effect of depositing CdSeTe and CdTe layers at different substrate temperatures (STs) by evaporation in vacuum on the properties of the CdSeTe/CdTe stacks was investigated. First, CdSeTe layers in stack structure were grown at STs of 150 °C, 200 °C and 250 °C and then CdTe layers on the CdSeTe produced with the optimum temperature were coated at STs of 150 °C, 200 °C and 250 °C. The employing of STs up to 150 °C on both CdSeTe and CdTe films in CdSeTe/CdTe stacks demonstrated the presence of Te and/or oxide phases as well as the alloying, while more stable phase structures at higher temperatures. In the CdSeTe/CdTe stack, the increase in ST of CdSeTe promoted the alloying, while it weakened the alloy in which was applied in CdTe. It was concluded that under the applied experimental conditions, STs of 250 °C and 200 °C with the graded alloying structure, suitable absorption sites, more homogeneous surface morphology for potential solar cell applications would be more suitable for CdSeTe and CdTe, respectively. As a result, the application of ST to CdSeTe or CdTe in the stacks can be used as a tool to control the properties of the stack structure.

Keywords: CdSeTe/CdTe, substrate temperature, interface, vacuum evaporation

1. Introduction

Polycrystalline CdTe has proven to be one of the most suitable materials for achieving highly efficient thin film solar cells due to its favorable optical properties and ease of manufacturing [1, 2]. Maturity of this solar cell technology is demonstrated by a cell efficiency of 22.1% and a photovoltaic (PV) module production volume of around 8 GW by the end of 2021 [3, 4]. The impressive increase in cell/-module efficiency during the last decade can be attributed to the inclusion of Se into the absorber or the junction partner in the cell configuration. Specifically, a significant contribution to device performance was obtained by placing a Cd(Se,Te) layer at the interface between the n-type window and the p-type CdTe absorber. This is because Cd(Se,Te) alloy

* Author to whom any correspondence should be addressed.

displays lower optical band gap value (∼1.40 eV) compared to CdTe (∼1.50 eV) and allows absorption of long wavelength photons (beyond 800 nm), thus increasing the short circuit-current. In one the study that focused on selenium graded CdSeTe/CdTe device had efficiency of 19.1% was exhibited. This device displayed open-circuit voltage (V_{OC}) of about 0.86 V comparable with the pure CdTe thin film based solar cell while enhancing the J_{SC} (short-circuit current density) from 26 to over 28 mA cm^{-2} [5]. In this context, the modified cell configuration can be obtained by; (i) depositing a Cd(Se,Te) layer between the n-type buffer (typically CdS) and the CdTe absorber layer [6], (ii) using a bi-layer junction partner (i.e. CdS/CdSe) that inter-diffuses with CdTe forming the Cd(Se,Te) interlayer during high-temperature deposition and treatment processes [7, 8].

In order to overcome the factors limiting the performance of the solar cells with Cd(Se,Te) interlayer, the studies were concentrated on the optimization of fabrication conditions such as their thickness, the effect of Cu doping on them, minority carrier lifetime, defect structure, $CdCl_2$ treatment, etc [9–15]. Among the existing conditions of fabrication, substrate temperature (ST) is an important parameter because it directly affects phase formation, grain size and conductivity of the CdSe and/or CdTe films as well as the quality of the interface at the CdSe/CdTe or Cd(Se,Te)/CdTe stacks [16–19]. In this context, in a very recent study examining the material and optical properties of CdSeTe thin films produced by close space sublimation (CSS) technique at various source and STs (in the range of 420–540), it has been reported that ST has significant effects on film crystallinity and grain growth [20]. Thus, it is vital to understand the behavior of the formation of the Cd(Se,Te)/CdTe interfaces such as the degree of alloying and film crystallinity formed at various STs.

Deposition methods play a critical role in the performance of the solar cells. In CdTe based solar cells, the CSS method has been intensively preferred recently [20–22]. However, evaporation method in vacuum allows more precise control of the thin Cd(Se,Te) layer and the roughness of the films compared to commonly used CSS and promises high efficiency. In a study, it was noted that CdSeTe/CdTe graded band gap solar cells produced by using vacuum evaporation method with an efficiency exceeding 19% can compete with sublimated polycrystalline CdTe thin film PVs as well [23].

This study aims to better understanding of the effect of the ST on interface formation for the CdSeTe/CdTe stacks produced by evaporation in vacuum. First, we report on the impact of ST (room temperature (RT), 150 °C, 200 °C and 250 °C) on the structural and optical properties of the CdSeTe layers. Then, to further elucidate the effect of the ST on interdiffusion, we form stacked samples comprising thin CdTe films deposited at different STs (150 °C–250 °C) onto the CdSeTe layers. In the second stage of the study, CdSeTe layer formed at 250 °C was selected based on the optimization results of the first step. Overall, we believe that ST can be used to increase the performance of devices by improving the interface of the junction.

2. Experimental details

To examine the effect of ST on CdSeTe/CdTe stacks, the samples were coated on soda lime glass (SLG) substrates. SLG substrates were washed in an ultrasonic cleaner using acetone, alcohol, deionized water and then dried with N_2 gas. CdSeTe and CdTe thin films were deposited using a quasi-closed setup by evaporation method in vacuum. The films were deposited at a vacuum level of 2×10^{-3} Pa using high purity source powders (99.99%) (see [24] for more details on the setup). To produce CdSeTe/CdTe stacks, CdSeTe alloys were first evaporated on SLG substrates and then CdTe layers were coated on the SLG/CdSeTe structure. CdSeTe alloys with 30% Se was used in all samples, due to previously optimized process. The reason of this ratio was to provide an optimum band gap of ∼1.4 eV.

The samples were organized in two groups based on different STs of the layers in the stack. The first group was CdSeTe/CdTe stacks in which the ST was not applied to CdTe, and the CdSeTe alloys were deposited at different STs. In the first group samples, CdSeTe thin films were deposited at STs of 150 °C, 200 °C and 250 °C. Then, CdTe layers were grown on SLG/CdSeTe structures. Based on the analysis results in first group, an ST of 250 °C was evaluated to be optimum for CdSeTe alloy deposition. Therefore, the second group samples were grown using a fixed ST of 250 °C for the CdSeTe thin films. CdTe thin films were then coated on the CdSeTe alloys at STs of 150 °C, 200 °C and 250 °C. CdSeTe and CdTe layers for all samples were grown at a source temperature of approximately 650 °C and the deposition rate of 1.5 nm s^{-1}. The thicknesses of CdSeTe and CdTe layers were set to 200 nm and 400 nm, respectively. Finally, all the stacks were annealed at 400 °C for 10 min in air atmosphere. The stacks obtained in this study are illustrated in figure 1.

Labels of CdSeTe/CdTe stacks produced at different STs are shown in table 1. In the table, CST and CT are abbreviations for CdSeTe and CdTe, respectively. For example, CST/CT label shows the stack for which no ST was applied during the deposition of CdSeTe and CdTe. The sample labeled CST(250)/CT shows that its CdSeTe was grown at the ST of 250 °C, and then CdTe was coated without applying any ST. Finally, CST(250)/CT(200) indicates that CdSeTe was produced at the optimum ST of 250 °C, and then CdTe was coated at an ST of 200 °C.

The thicknesses of the stacks were measured with DektakXT stylus profilometer. X-ray diffraction (XRD) spectra were acquired with a Rigaku SmartLab diffractometer in $2\theta = 20°-60°$ range. Raman and photoluminescence spectra were carried out with a Renishaw confocal Raman microscope at 633 nm. The surface images of the stacks were obtained with Zeiss EVO LS10 SEM. Atomic ratios were determined with Oxford Instruments EDS attachment. Transmittance curves were provided with Dongwoo Optron UV–Vis spectrophotometer.

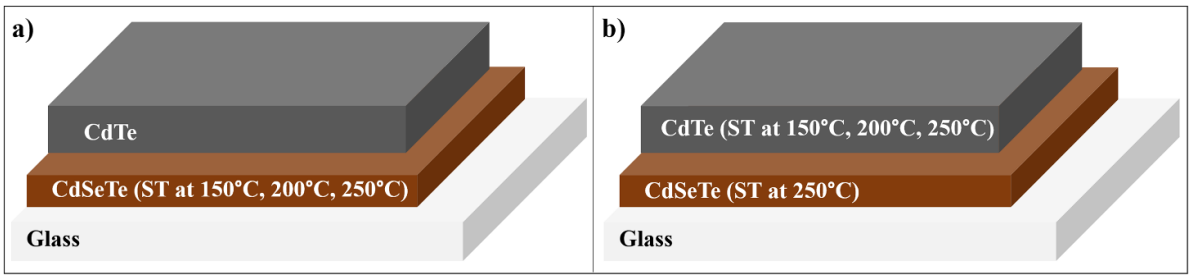

Figure 1. Schematic representation of CdSeTe/CdTe stacks obtained depending on substrate temperature (ST) of (a) CdSeTe, (b) CdTe.

Table 1. Labels of CdSeTe/CdTe stacks deposited at different substrate temperature ('ST' and 'RT' refer to substrate temperature and room temperature, respectively).

ST of CdSeTe	ST of CdTe	Labels of the samples
RT	RT	CST/CT
150 °C	RT	CST(150)/CT
200 °C	RT	CST(200)/CT
250 °C	RT	CST(250)/CT
250 °C	150 °C	CST(250)/CT(150)
250 °C	200 °C	CST(250)/CT(200)
250 °C	250 °C	CST(250)/CT(250)

3. Results and discussion

3.1. CdSeTe/CdTe stacks obtained with CdSeTe layers deposited at different STs

The XRD spectra of the CdSeTe/CdTe samples in which CdSeTe layers have been grown in the ST range of 150 °C–250 °C are shown in figure 2. In the CST/CT stack deposited without applying ST, a multi-phase structure occurred. The comparison of the peak positions with database revealed the presence of cubic CdSe phase (PDF#00-019-0191) and cubic $CdSe_xTe_{1-x}$ alloy with low Se-ratio ($x \sim 0.09$) in the sample. The Se-ratio in the alloy was calculated based on Vegard's law. In addition, formations of a Te phase crystallizing in hexagonal structure (PDF#00-002-0511) and the $CdTeO_3$ oxide phase (PDF#00-022-0129) were also detected. Growth of the CdSeTe layer at an ST of 150 °C resulted in a more dominant $CdSe_xTe_{1-x}$ alloy ($x \sim 0.23$) compared to the sample without ST. However, while the cubic CdSe phase disappeared, Te phase was also present in this sample. It was also noted that the structure of the oxide phase changed and turned into monoclinic $CdSeO_3$ phase (PDF#00-051-0155). Increasing the ST of the CdSeTe film to 200 °C led to a significant change in the phase structure of the stack. It was determined that CdTe (PDF#00-015-0770) and $CdSe_xTe_{1-x}$ alloy ($x \sim 0.31$) crystallized in cubic structure in this sample. ST of 250 °C for CdSeTe film did not cause any change in the crystal structure of CdSeTe and CdTe. However, two CdSeTe alloys with different Se-concentration were formed, as seen in figure 3. It was determined that a graded alloy structure with $CdSe_xTe_{1-x}$ ($x \sim 0.31$) and $CdSe_yTe_{1-y}$ ($y \sim 0.04$) was formed. In the light of these results;

(i) Despite using a CdSeTe source with approximately 30% Se-ratio only an alloy with low concentration of Se was preserved in the CST/CT structure. However, applying the ST during growth resulted in an increase in the Se content in the alloy. This points out that applying ST during CdSeTe layer growth plays an effective role in decreasing/limiting the Se diffusion.

(ii) In the CST/CT sample, cubic CdSe was formed as a result of phase separation of the CdSeTe alloy during deposition or post-deposition treatments. However, the cubic crystallization of CdSe instead of the stable hexagonal phase may be due to the dominant cubic nature of the stack structure itself. However, the fact that no phase formation related to CdSe is observed at 200 °C and 250 °C of CdSeTe implies that a minimum temperature of 200 °C should be applied to prevent phase segregation in the stack structure.

(iii) $CdTeO_3$ and $CdSeO_3$ oxide phases were formed in the CST/CT and CST(150)/CT stacks due to the annealing effect in air atm. Oxidation can occur during annealing in the air atmosphere of CdSeTe/CdTe stack. In this context, the main oxidation product such as $CdTeO_3$ is formed due to the reaction of CdTe and oxygen [25]. However, the absence of oxide and Te phases at temperatures higher than 150 °C shows that applying a certain ST can assist in preventing formation of oxide phases and elemental tellurium.

(iv) The phase diagram of CdTe shows that CdTe and elemental phases can coexist in stoichiometric deviations. The graph of phase diagram says that temperatures above 450 °C are the solidification line of the Te phase [26]. In this context, the formation of the Te phase seen in CST/CT and CST(150)/CT samples is possible under the applied experimental conditions. Elemental Te may result from the decomposition of CdTe, which has a higher melting point than the annealing temperature, where slurry mixtures of CdTe and oxides have been observed [27]. However, the disappearance of the Te-phase at STs higher than 150 °C for CdSeTe growth indicates that there is a minimum ST that must be applied under the experimental conditions to prevent the formation of elemental Te-phase.

A graded alloy structure of CdSeTe is generally preferred to improve solar cell performance. This only happened at an ST of 250 °C. Therefore, grazing incidence (GI-XRD) spectra were taken to detect the phase distribution through the film

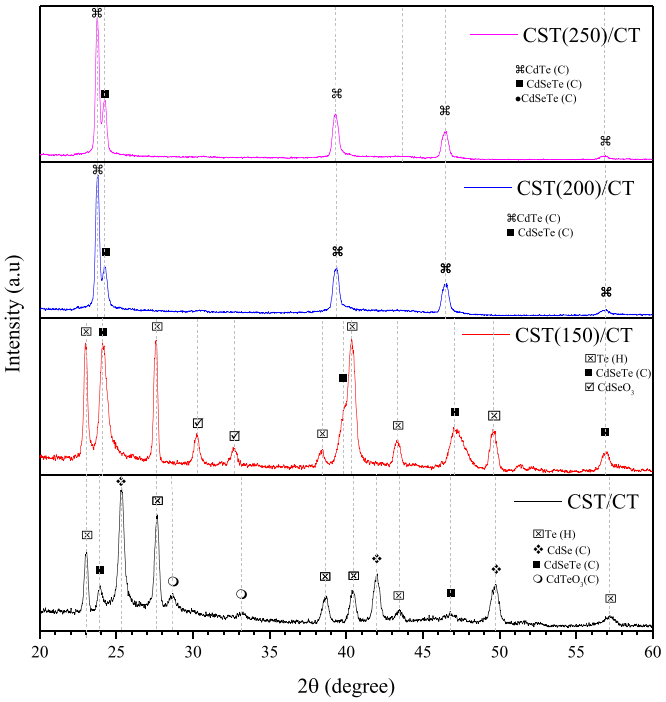

Figure 2. XRD spectra of CdSeTe/CdTe stacks in which CdSeTe thin films were deposited at different substrate temperature ('C' and 'H' denote cubic and hexagonal structure).

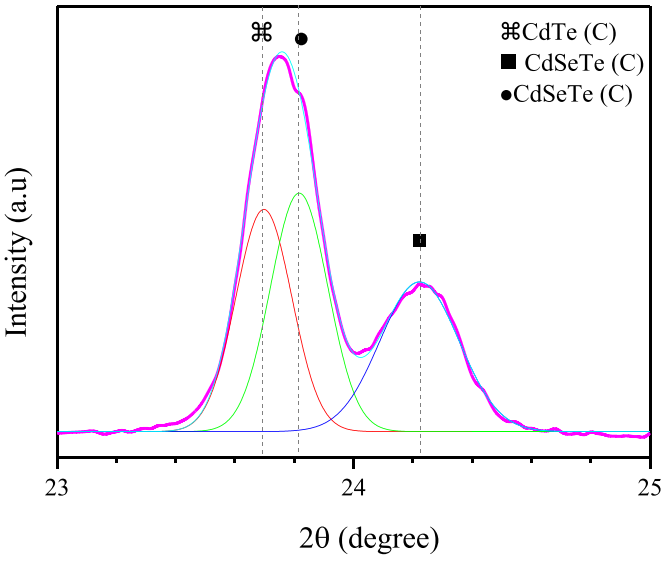

Figure 3. Expanded XRD spectra of CST(250)/CdTe stacks.

depth. GI-XRD spectrum of the sample at 250 °C are shown in figure 4. The estimated x-ray penetration thicknesses for GI-XRD measurement at incidence angles of 0.5°, 1° and 3° are about 50 nm, 110 nm and 350 nm, respectively. It can be seen from the figure that the spectra at 0.5° and 1° taken from the near-surface region indicate weak crystallization. In addition, 0.5° data revealed that $CdSe_xTe_{1-x}$ ($x \sim 0.03$) and $CdSe_yTe_{1-y}$ ($y \sim 0.33$) alloys crystallized in cubic structure with two different Se-compositions. It was also determined that a Te-rich cubic CdTe phase also formed. The presence of this phase

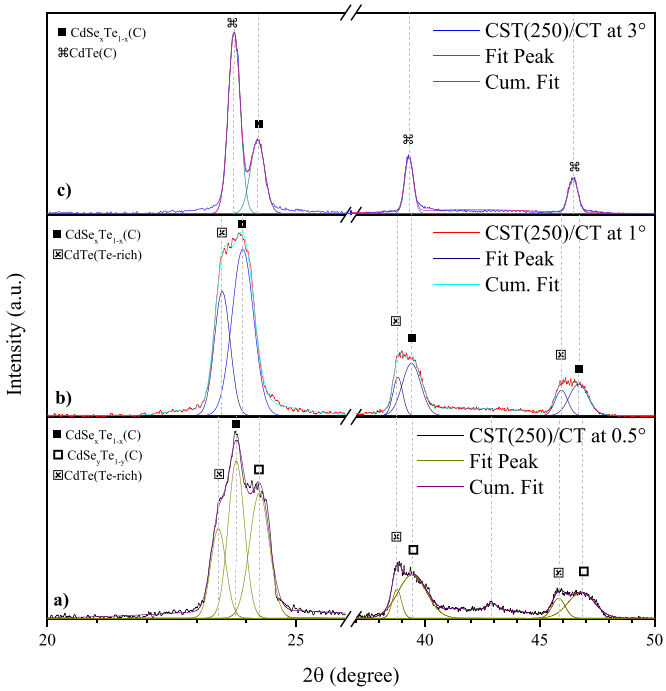

Figure 4. GI-XRD spectra of CST(250)/CT stack at (a) 0.5°, (b) 1.0° and (c) 3°.

structure was detected by the fact that the lattice parameter for this phase ($a_o = 6.566$ Å) was higher than the lattice parameter of CdTe ($a_o = 6.481$ Å) [28]. It was observed that there was a weakening in the gradual alloying of CdSeTe with the increase of the incidence angle to 1°. Matching of peak positions indicated presence of a single $CdSe_xTe_{1-x}$ (x ∼ 0.11) alloy and a Te-rich CdTe phase. Data collected at the incidence angle of 3° correspond to the bulk of the film and it indicates that $CdSe_xTe_{1-x}$ ($x \sim 0.31$) and CdTe phases dominate the spectra.

GI-XRD results show that the Se-concentration is more intense in the near-surface region. It can be said that the reason for this is the rapid diffusion of Se toward the film surface during deposition and post-annealing processes.

Raman spectra of the CdSeTe/CdTe stacks produced by changing the ST during CdSeTe growth are shown in figure 5. In order to designate the phase structure in the Raman spectrum, it is useful to define the Raman mode positions of the CdTe, CdSe and Te phases, which also appear in the XRD spectra. In this sense, CdTe at 139 (TO), 164 (LO) and 328 (2LO) cm^{-1}; CdSe at 206 (LO) and 412 (2LO) cm^{-1} and Te at 94 (E_1), 122 (A_1) and 142 (E_2) cm^{-1} have mode positions [16, 29–32].

In the Raman spectrum of the CST/CT sample without the ST, while the strong Raman peak at 122 cm^{-1} corresponds to the A_1 mode of Te phase; the peak at 204 cm^{-1} corresponds to the LO mode of CdSe. The Raman mode at 139 cm^{-1} located in the same spectrum belongs to the TO mode of CdTe and E_2 mode of Te. Growing CdSeTe at an ST of 150 °C favored the reformation of the dominant CdTe phase (TO mode 138 cm^{-1}) and the CdSeTe alloy (TO mode 156 cm^{-1}), while the modes corresponding to CdSe and Te disappeared. Growing CdSeTe

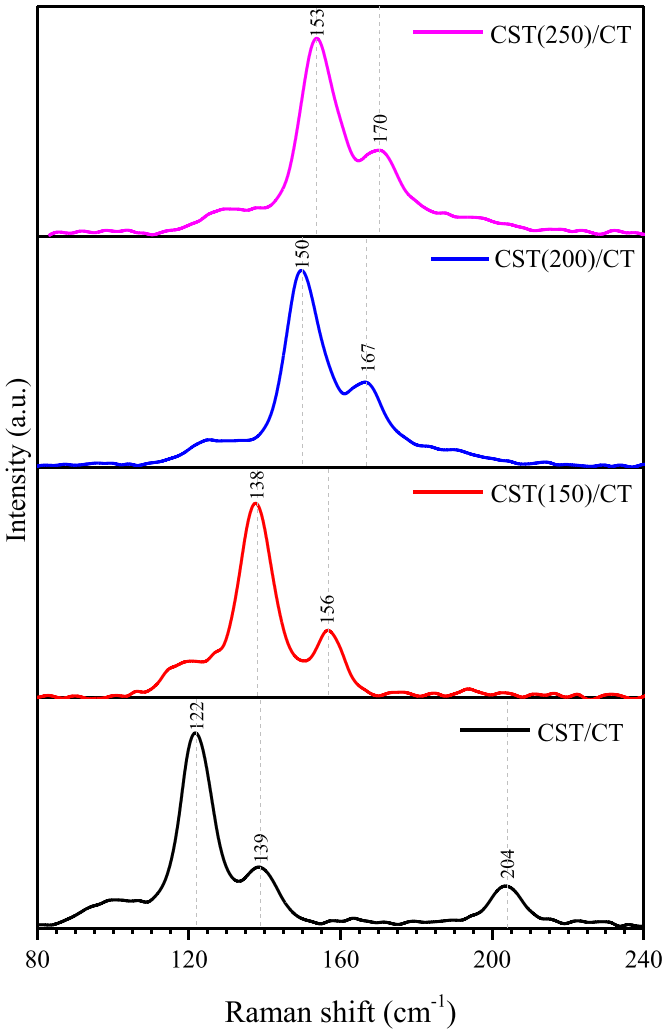

Figure 5. Raman spectra of CdSeTe/CdTe stacks in which CdSeTe thin films were deposited at different substrate temperature.

at an ST of 200 °C resulted in a significant rightward shift of the Raman peaks compared to the 150 °C data. Examination of the peak positions revealed the prominent TO mode of CdSeTe alloy at 150 cm^{-1} and the LO mode of CdTe at 167 cm^{-1}. An increase in the ST to 250 °C caused the Raman peaks to shift slightly to the right. This indicates a marked increase in Se content in phases. It can be said that the results obtained with Raman modes are generally consistent with the XRD spectra results. Some differences in phase structures are due to data collection from the near-surface region of Raman instrument.

Especially in thin-layered structures, surface morphologies play an important role in device performance [33]. In order to examine the grain structures, SEM images of the stacks in which CdSeTe is deposited in the ST range of 150 °C–250 °C are shown in figure 6. CST/CT sample has a pinhole-free, dense, partially inter-granular voids. The grain size of the sample with a large-small grain structure varies in the range of 100–200 nm. The deposition of CdSeTe at an ST of 150 °C in the stack structure caused the grains to transform into a compact surface morphology and increased grain size (120–400 nm range). Increasing the ST to 200 °C did not cause a significant change in the surface structure of the stack, except for partial growth of some grains. However, increasing the ST to 250 °C caused a more homogeneous grain distribution in the stack. It was observed that the grain size decreased to the range of 130–250 nm. In this context, it can be said that Se is more involved in the CdTe structure and passivates the critical defects [34]. This is consistent with the XRD data at an ST of 250 °C, showing a gradual alloying of Se with CdTe.

The transmittance spectra of the CdSeTe/CdTe stacks are shown in figure 7. Although CdSeTe and CdTe films have strong absorption characteristic, this data displays high transmittance for all samples due to the fact that the stacks are much thinner than what is generally used in solar cell structures. It can be seen that the CST/CT sample has an absorption edge at around 725 nm (∼1.71 eV) corresponding to CdSe, and around 867 nm (∼1.43 eV) corresponding to CdSeTe alloy. For the 150 °C sample, the absorption edges shifted to larger wavelengths (hence smaller energies), implying existence of Se-rich $CdTe_zSe_{1-z}$ (∼1.56 eV) alloy at 794 nm and Te-rich $CdSe_xTe_{1-x}$ (∼1.45 eV) alloy at 856 nm. Increasing the ST further made the absorption transitions sharper, probably due to the improvement of crystallization. In the 200 °C and 250 °C samples, absorption edge of the Te-rich $CdSe_xTe_{1-x}$ alloy shifted to about 890 nm (∼1.39 eV), while the absorption edge of the Se-rich $CdTe_zSe_{1-z}$ alloy did not change (∼795 nm).

The changes observed in the absorption edges of the samples indicate that application of ST during growth of the CdSeTe layer of the stack promotes alloying. The increase in ST supported the transition of the absorption edge toward the optimum band gap by increasing the alloy grade.

Photoluminescence (PL) measurements at RT were carried out to examine the defect states of the CdSeTe/CdTe stacks. The PL spectra of the stacks in which CdSeTe layers are produced at various STs, and the corresponding fitting results are shown in figure 8. The CST/CT sample has a Gaussian emission peak at 726 nm that corresponds to the transition of CdSe [35]. There are also transitions corresponding to $CdSe_xTe_{1-x}$ alloys with different Se-ratios at 811 nm and 951 nm. While the band emission of CdSe disappears at the ST of 150 °C, there are PL emissions corresponding to the band-transition of CdTe and CdSeTe at 818 and 870 nm. Emission bands at 817 and 821 nm in the PL spectrum of the sample at 200 °C may be phonon replicas of CdTe [36]. Also, the peak appearing at 888 nm represents the transition of the CdSeTe alloy. In the 250 °C ST of CdSeTe, CdTe has PL band emission at 821 nm. In addition, the graded structure represents the band emissions of Te-rich CdSeTe alloys with different Se-ratio at 833 and 903 nm, respectively.

3.2. CdSeTe/CdTe stacks in which CdTe was deposited at different STs

The XRD spectra of the CdSeTe/CdTe stacks in which CdTe layers were produced at STs in the range of 150 °C–250 °C are shown in figure 9. In the stacks where CdTe was

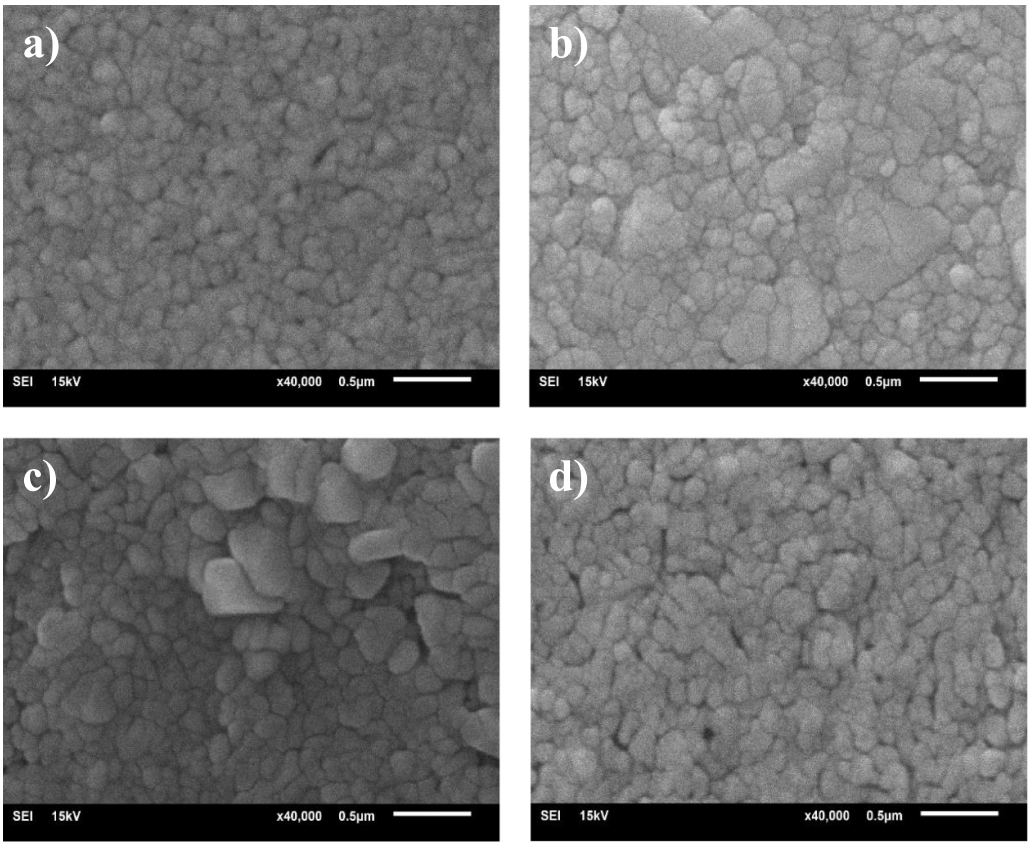

Figure 6. SEM images of (a) CST/CT, (b) CST(150)/CT, (c) CST(200)/CT, (d) CST(250)/CT samples.

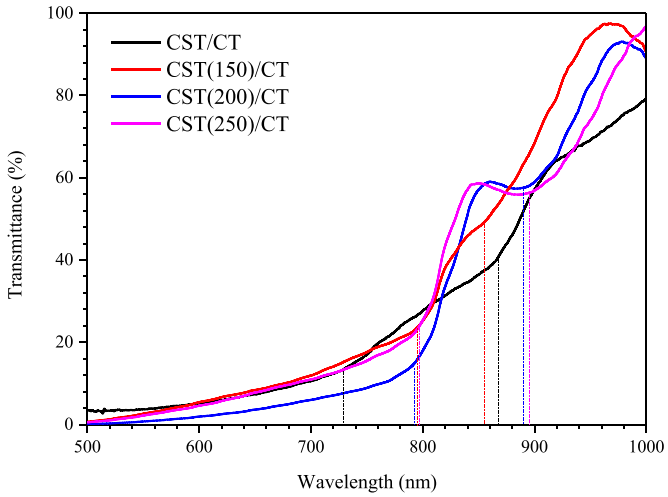

Figure 7. Transmittance spectra of CdSeTe/CdTe stacks in which CdSeTe thin films were deposited at different substrate temperature.

producedat 150 °C and 200 °C, it was observed that some peaks overlapped with poor crystallization. Therefore, deconvolution was used and results are also shown on the spectrum. The results of CST(250)/CT(150) stack showed the presence of CdTe and $CdSe_xTe_{1-x}$ alloy ($x \sim 0.26$) in cubic crystal structures. In addition, it was determined that hexagonal Te phase formed in the same sample (PDF#00-002-0511). In the CST/CT(200) sample in which CdTe is produced at an ST of 200 °C, elemental Te phase disappeared, CdTe and $CdSe_xTe_{1-x}$ ($x \sim 0.23$) phases crystallized in cubic structure. Increasing the CdTe ST to 250 °C caused the Se-related phases in the stack structure to disappear and a strong CdTe phase dominated the data.

Considering the phase formation of the stacks, it is seen that the increase in the ST of CdTe leads to the disappearance of the graded alloy structure. In addition, based on the peak intensities and full width at half maximum (FWHM) values, the phase of the CdSeTe alloy is more dominant than CdTe at 150 °C, while the CdTe phase is more prominent than the CdSeTe alloy at 200 °C.

According to the GI-XRD results taken at 0.5° and shown in figure 10, the stack in which the CdTe layer was produced at an ST of 200 °C, has a $CdSe_xTe_{1-x}$ ($x \sim 0.29$) alloy and Te-rich cubic CdTe phase. Also, TeO_3 phase was observed close to the surface (PDF#00-022-0911). Increasing the incident angle to 1° caused a significant change in the observed phase structure, leading to the emergence of a hexagonal CdSe phase and a significant decrease in the amount of Se in the $CdSe_xTe_{1-x}$ alloy ($x \sim 0.09$). In addition, although TeO_3 and Te-rich CdTe phases appeared, it was determined that these phases were weakened. Data collected at 3° showed only cubic CdTe and $CdSe_xTe_{1-x}$ alloy ($x \sim 0.26$).

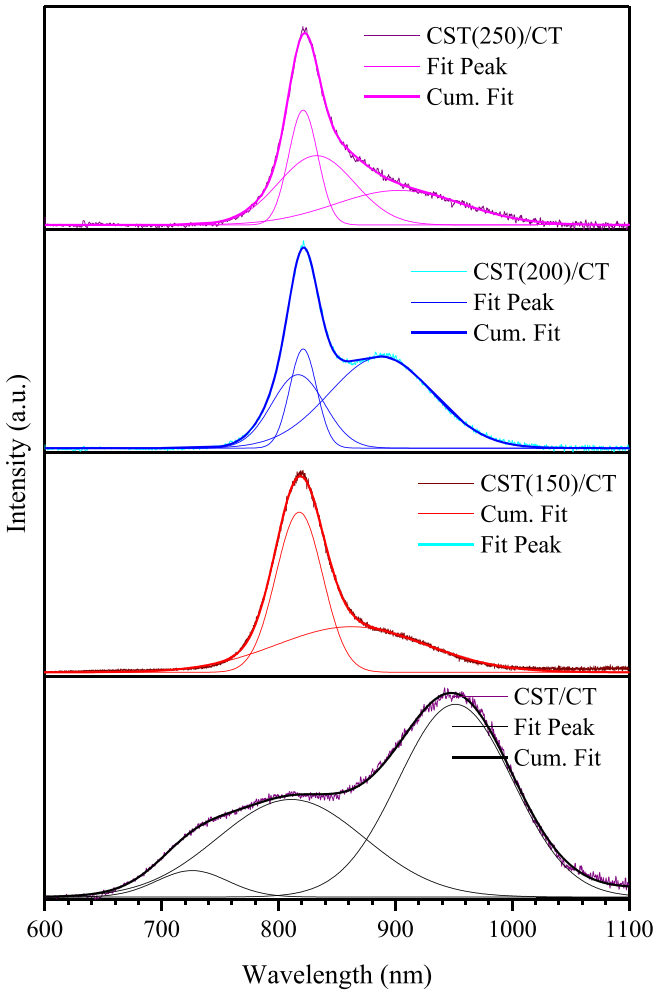

Figure 8. Photoluminescence spectra of CdSeTe/CdTe stacks in which CdSeTe thin films were deposited at different substrate temperature.

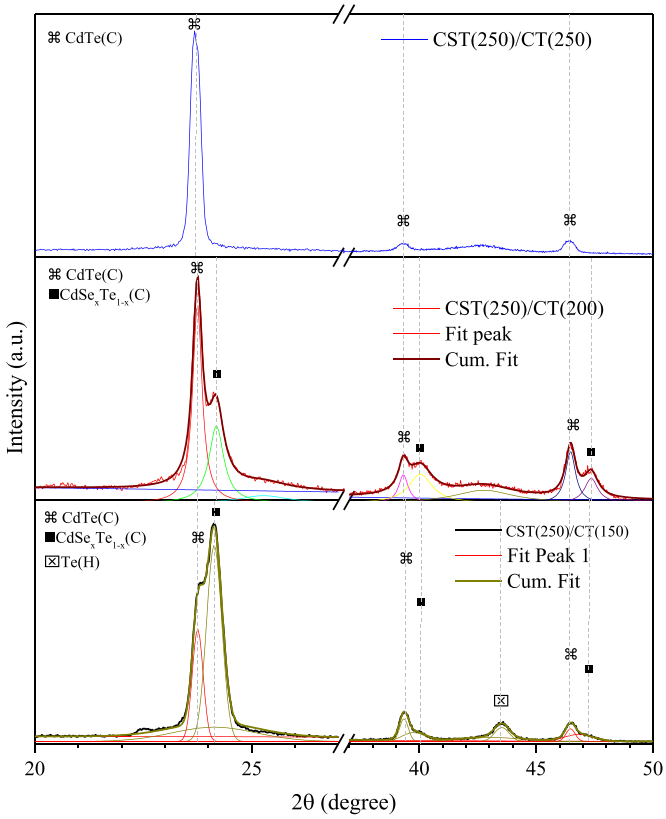

Figure 9. XRD spectra of CdSeTe/CdTe stacks in which CdTe thin films were deposited at different substrate temperature.

The GI-XRD results of the sample produced at 200 °C showed the presence of a higher Se-rate alloy in the near-surface region, while a relatively weaker alloy was observed in the bulk.

The Raman spectra of the stacks produced by changing the ST during CdTe growth and the fitting results corresponding to these spectra are shown in figure 11. The Raman spectrum of the stack in which CdTe was produced at an ST of 150 °C showed a graded phase structure. In this context, the peak at 108 cm^{-1} to the right of the E_1 mode of Te phase (at 94 cm^{-1}) suggests that this may belong to non-stoichiometric CdTe structure with a high Te-content. The Raman peaks at 169 and 335 cm^{-1} correspond to the LO and 2LO modes of $CdSe_xTe_{1-x}$ alloy with the rather small Se-ratio, while the peaks at 177 and 342 cm^{-1} belong to the LO and 2LO modes of the relatively low Se-ratio $CdSe_yTe_{1-y}$ alloy. It can be said that the Raman peak at 189 cm^{-1} corresponds to the LO mode of the $CdSe_zTe_{1-z}$ alloy with the highest Se-ratio in the sample. Increasing the ST of CdTe to 200 °C did not cause a significant change in the phase structure except for the slight shift in the Se-concentrations of the CdSeTe alloys. An ST of 250 °C caused the graded structure to begin to weaken. However, the peaks at 170 and 173 cm^{-1} correspond to the LO mode of CdSeTe alloy with the rather low Se-ratio.

Raman spectra of the samples in which CdSeTe was produced at a constant ST (250 °C) and CdTe in the range of 150 °C–250 °C showed that the phase structure formed a graded $CdSe_xTe_{1-x}$ alloy with varying Se-ratio. However, the highest ratio of alloy structure is exhibited at 200 °C. The weakening of the alloy at 250 °C implies that there is an ST limit for CdTe deposition under the applied experimental conditions.

SEM images of CdSeTe(250)/CdTe stacks in which CdTe was produced at STs in the range of 150–250 are presented in figure 12. It was observed that the polycrystalline CST(250)/CT(150) sample in which CdTe was produced at an ST of 150 °C had a homogeneous, granular structure with sizes in the 100–200 nm range. It can be said that this small-grained structure is probably due to the incorporation of more Se into the structure compared to other samples. Increasing the ST of CdTe to 200 °C resulted in a clustered structure in the surface morphology of the stack, in which smaller grains came together to form larger grains. While this led to coarse grained structures, a significant reduction in inter-granular voids was also observed. As the ST increased to 250 °C for CdTe, a

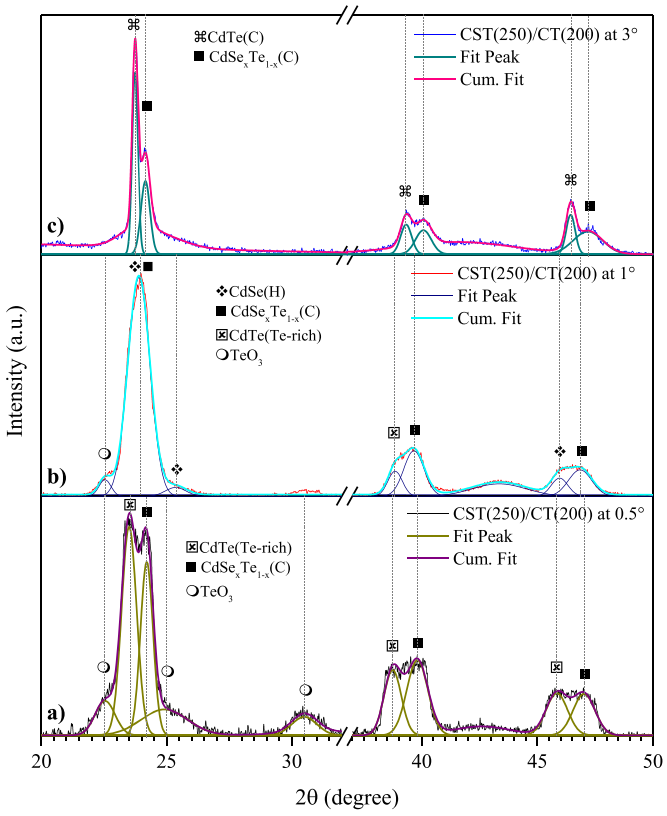

Figure 10. GI-XRD spectra of CST(250)/CT(200) stack at (a) 0.5°, (b) 1.0° and (c) 3°.

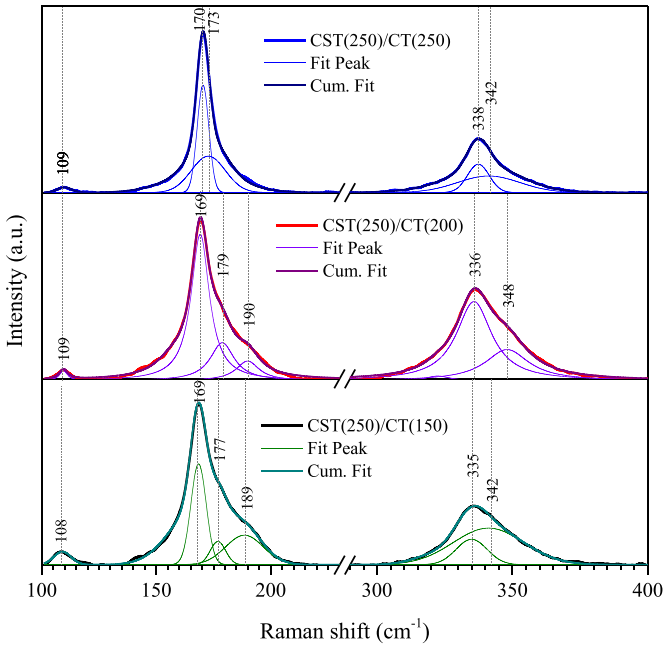

Figure 11. Raman spectra of CST(250)/CT stacks in which CdTe were coated at different substrate temperature.

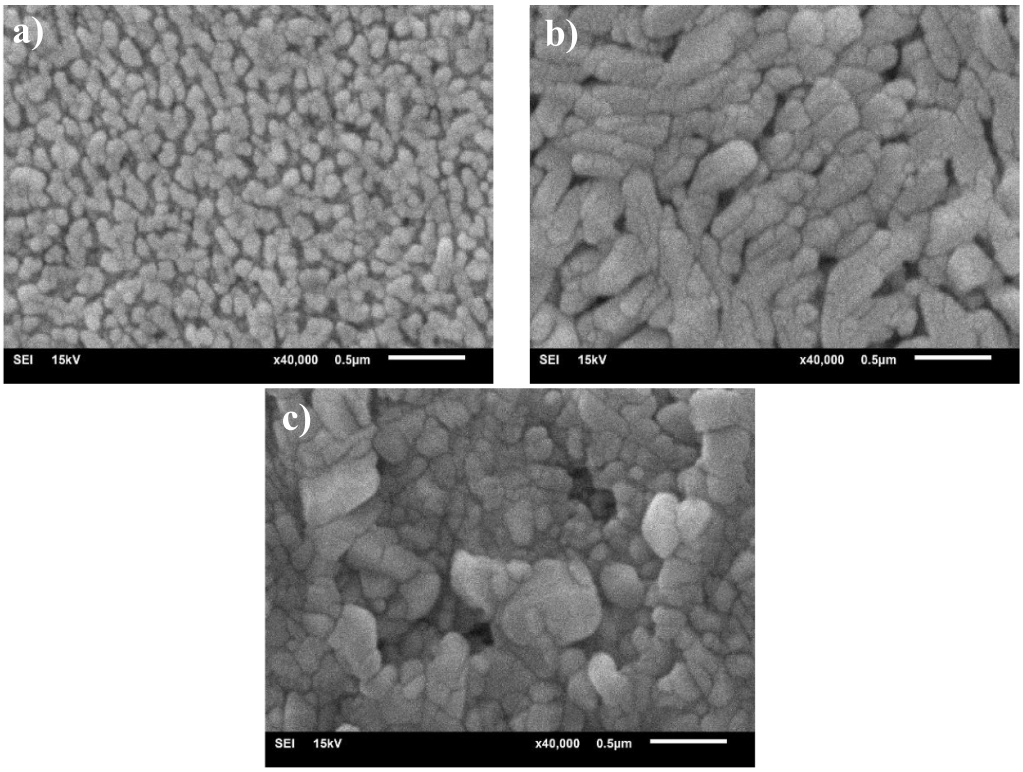

Figure 12. SEM images of (a) CST(250)/CT(150) (b) CST(250)/CT(200) (c) CST(250)/CT(250).

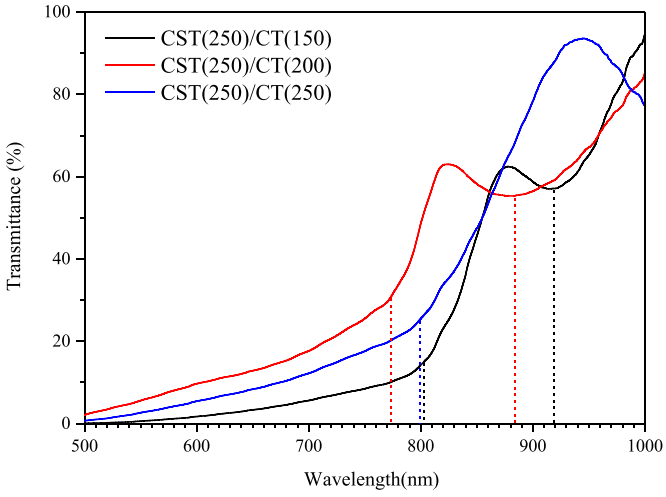

Figure 13. Transmittance curves of CST(250)/CT stacks in which CdTe were coated at different substrate temperature.

denser and rougher structure was formed. It was noted that a large-small grain structure was formed with sizes in the 200–600 nm range. This grain structure may indicate the presence of less Se in the alloys compared to other samples. This was consistent with the XRD results of the samples.

The transmittance curves of the samples of figure 12 are shown in figure 13. Deposition of CdTe at the ST of 150 °C led to the formation of absorption edges at 803 nm and 919 nm, corresponding to Se-rich $CdTe_zSe_{1-z}$ and Te-rich $CdSe_xTe_{1-x}$ alloys. As the substrate temperature increased to 200 °C, it was determined that the absorption transition shifted to 773 nm and 884 nm, indicating a decrease in the Se-content of the alloys. However, the 250 °C data showed an absorption edge at only 799 nm, indicating the disappearance of the gradual alloy structure. The results obtained with the absorption transitions of the samples were consistent with the XRD results.

Photoluminescence spectra of CdSeTe(250)/CdTe stacks are shown in figure 14. The positions of the PL emission bands for the 150 °C sample are at around 813 nm and 859 nm. It can be said that these peaks belong to Se-rich $CdTe_zSe_{1-z}$ alloy

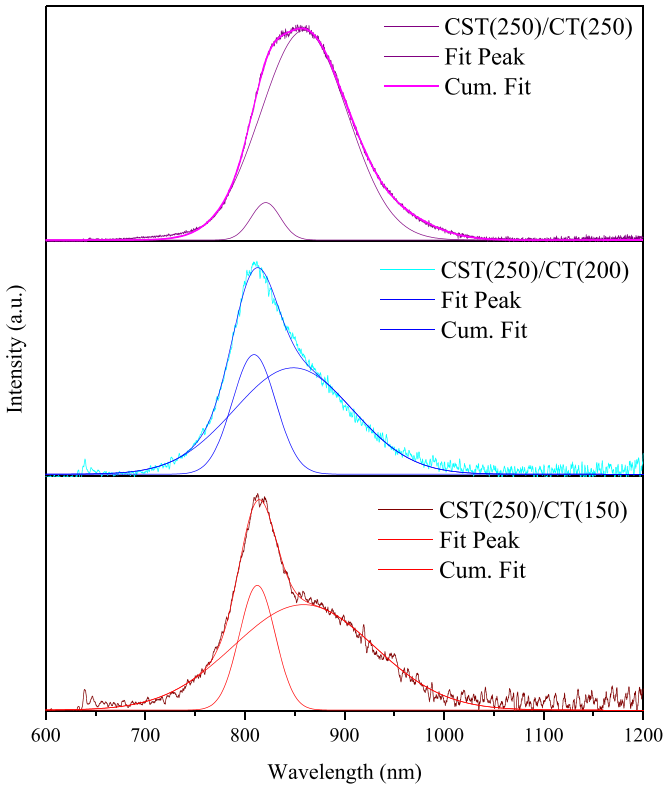

Figure 14. Photoluminescence spectra of CdSeTe/CdTe stacks in which CdTe thin films were deposited at different substrate temperature.

and Te-rich $CdSe_xTe_{1-x}$ alloy, respectively. It was observed that the Se-rich and Te-rich phases shifted slightly to the left (hence to higher energies) (809 and 849 nm) when the S was increased to 200 °C. However, when the temperature increased to 250 °C, it was determined that PL peaks were at 816 nm and 854 nm, shifting slightly to the right. Considering the intensities of the peaks and FWHM values, no significant difference was observed in the PL spectra at 150 °C and 200 °C. In these samples, the Se-rich phase appeared more dominantly than the Te-rich phase. In the 250 °C sample, it was observed that the Te-rich phase was formed strongly.

4. Conclusions

The effect of depositing CdSeTe and CdTe layers at different STs on the structural and optical properties in CdSeTe/CdTe stacks was investigated. CdSeTe and CdTe layers in stacks were deposited by evaporation in vacuum at the STs of 150 °C, 200 °C and 250 °C. XRD results of the samples with CdSeTe layer produced by various STs showed that a relatively weak alloying of CdSeTe, undesired metallic Te and oxide phases formed at STs up to 150 °C. It was noted that the alloying strengthened (Se-ratio up to 31%) and strange phases did not occur at the STs of CdSeTe higher than 150 °C. The Raman spectra substantially supported the XRD results with some differences. Surface images of the stacks confirmed that the Se-ratio in the alloy increased with increment of ST. Transmittance and PL spectra revealed the presence of absorption transition and emission bands of alloys with different-Se ratio depending on the STs of CdSeTe in stacks. Analysis results suggested that the optimum ST for CdSeTe might be 250 °C and therefore, CdSeTe layers were grown at 250 °C to investigate the effect of growing CdTe at various STs on CdSeTe/CdTe stacks.

Growing CdTe at an ST of 150 °C exhibits the formation of the elemental Te phase together with the CdTe and CdSeTe alloy; the deposition of CdTe at 200 °C caused the elemental Te-phase to disappear. However, the 250 °C ST of CdTe showed the dominant cubic CdTe phase that the alloying in the stack disappeared. Raman spectra demonstrated that alloying could occur in all CdSeTe/CdTe stacks produced at different STs of CdTe. However, it also confirmed that the weakest graded structure could be at 250 °C. SEM images promoted that the alloying decreased as the ST of CdTe increased. Transmittance spectra suggested a graded structure at 150 °C and 200 °C of CdTe, while only a single phase was present at 250 °C.

Overall, the results show that ST can be applied in the deposition of CdSeTe and CdTe layers to improve the characteristics of CdSeTe/CdTe stacks. It was concluded that under the applied experimental conditions, an ST of 250 °C for CdSeTe and 200 °C for CdTe would be more suitable for potential solar cell applications.

Data availability statement

Data will be made available on request.

The data cannot be made publicly available upon publication because no suitable repository exists for hosting data in this field of study. The data that support the findings of this study are available upon reasonable request from the authors.

Acknowledgments

The authors would like to thank Dr Bülent M Başol for valuable support in editing the manuscript.

Authorship contribution statement

Ali Çiriş: Conceptualization, Methodology, Writing—original draft, Writing—review & editing.

Yavuz Atasoy: Conceptualization, Methodology, Writing—original draft.

Murat Tomakin: XRD, SEM, EDS and Optical characterizations.

Abdullah Karaca: Sample preparation.

Tayfur Küçükömeroğlu: Sample preparation.

Emin Bacaksız: Conceptualization and review & editing.

Conflict of interest

The author declares that he has no known competing financial interests or personal relationships that could have appeared to influence the work reported in this paper.

ORCID iDs

Ali Çiriş https://orcid.org/0000-0003-4266-2080
Abdullah Karaca https://orcid.org/0000-0001-5001-5559
Emin Bacaksız https://orcid.org/0000-0002-0041-273X

References

[1] Scarpulla M A, McCandless B, Phillips A B, Yan Y, Heben M J, Wolden C, Xiong G, Metzger W K, Mao D and Krasikov D 2023 CdTe-based thin film photovoltaics: recent advances, current challenges and future prospects *Sol. Energy Mater. Sol. Cells* **255** 112289

[2] Hasani E and Raoufi D 2021 Comprehensive study of physical properties of cadmium telluride thin films: effect of post-deposition high annealing temperature *Semicond. Sci. Technol.* **36** 055004

[3] Green M A, Dunlop E D, Siefer G, Yoshita M, Kopidakis N, Bothe K and Hao X 2023 Solar cell efficiency tables (Version 61) progress in photovoltaics: research and applications **31** 3–16

[4] Fraunhofer ISE 2022 *Photovoltaics Report* Fraunhofer Institute for Solar Energy Systems

[5] Munshi A H, Kephart J, Abbas A, Raguse J, Beaudry J-N, Barth K, Sites J, Walls J and Sampath W 2017 Polycrystalline CdSeTe/CdTe absorber cells with 28 mA cm^{-2} short-circuit current *IEEE J. Photovolt.* **8** 310–4

[6] Çiriş A, Başol B M, Atasoy Y, Karaca A, Tomakin M, Küçükömeroğlu T and Bacaksız E 2022 Effect of ultra-thin $CdSe_xTe_{1-x}$ interface layer on parameters of CdTe solar cells *Sol. Energy* **234** 128–36

[7] Paudel N R and Yan Y F 2014 Enhancing the photo-currents of CdTe thin-film solar cells in both short and long wavelength regions *Appl. Phys. Lett.* **105** 183510

[8] Yang X Y, Liu B, Li B, Zhang J Q, Li W, Wu L L and Feng L H 2016 Preparation and characterization of pulsed laser deposited a novel CdS/CdSe composite window layer for CdTe thin film solar cell *Appl. Surf. Sci.* **367** 480–4

[9] Lingg M, Spescha A, Haass S G, Carron R, Buecheler S and Tiwari A N 2018 Structural and electronic properties of $CdTe_{1-x}Se_x$ films and their application in solar cells *Sci. Technol. Adv. Mater.* **19** 683–92

[10] Bastola E, Phillips A B, Barros-King G, Jamarkattel M K, D-b Li, Quader A, Pokhrel D, Gibbs J M, Yan Y and Ellingson R J 2021 Understanding the Interplay between CdSe Thickness and Cu Doping Temperature in CdSe/CdTe Devices *2021 IEEE 48th Photovoltaic Specialists Conf. (PVSC)* (https://doi.org/10.1109/PVSC43889.2021.9518832) (IEEE)

[11] McGott D L, Good B, Fluegel B, Duenow J N, Wolden C A and Reese M O 2021 Carrier lifetime as a function of Se content for CdSexTe1-x films grown on Al2O3 and MgZnO *2021 IEEE 48th Photovoltaic Specialists Conf. (PVSC)* (https://doi.org/10.1109/PVSC43889.2021.9518914) (IEEE)

[12] Shah A, Pandey R, Nicholson A, Lustig Z, Abbas A, Danielson A, Walls J, Munshi A and Sampath W 2021 Understanding the role of CdTe in polycrystalline $CdSe_xTe_{1-x}$/CdTe-graded bilayer photovoltaic devices *Sol. RRL* **5** 2100523

[13] Guo J, Mannodi-Kanakkithodi A, Sen F G, Schwenker E, Barnard E, Munshi A, Sampath W, Chan M K and Klie R F 2019 Effect of selenium and chlorine co-passivation in polycrystalline CdSeTe devices *Appl. Phys. Lett.* **115** 153901

[14] Xiao C, Jiang C-S, Nardone M, Albin D, Danielson A, Munshi A H, Shimpi T, Sampath W, Jones S and Al-Jassim M M 2022 Microscopy visualization of carrier transport in CdSeTe/CdTe solar cells *ACS Appl. Mater. Interfaces* **14** 39976–84

[15] Munshi A H, Kephart J M, Abbas A, Danielson A, Gélinas G, Beaudry J-N, Barth K L, Walls J M and Sampath W S 2018 Effect of $CdCl_2$ passivation treatment on microstructure and performance of CdSeTe/CdTe thin-film photovoltaic devices *Sol. Energy Mater. Sol. Cells* **186** 259–65

[16] de Moure-flores F, Quiñones-Galván J, Guillén-Cervantes A, Arias-Cerón J, Hernández-Hernández A, Santoyo-Salazar J, Santos-Cruz J, Mayén-Hernández S, Olvera M and Mendoza-Álvarez J 2014 CdTe thin films grown by pulsed laser deposition using powder as target: effect of substrate temperature *J. Cryst. Growth* **386** 27–31

[17] Bacaksiz E, Basol B, Altunbaş M, Novruzov V, Yanmaz E and Nezir S 2007 Effects of substrate temperature and post-deposition anneal on properties of evaporated cadmium telluride films *Thin Solid Films* **515** 3079–84

[18] Hu P, Li B, Feng L, Wu J, Jiang H, Yang H and Xiao X 2012 Effects of the substrate temperature on the properties of CdTe thin films deposited by pulsed laser deposition *Surf. Coat. Technol.* **213** 84–89

[19] Bao Z, Yang X, Li B, Luo R, Liu B, Tang P, Zhang J, Wu L, Li W and Feng L 2016 The study of CdSe thin film prepared by pulsed laser deposition for CdSe/CdTe solar cell *J. Mater. Sci., Mater. Electron.* **27** 7233–9

[20] Danielson A, Reich C, Drayton J, Bothwell A, Shimpi T, Sites J and Sampath W 2023 A comprehensive material

study of CdSeTe films deposited with differing selenium compositions *Thin Solid Films* **768** 139684
[21] Hu A, Zhou J, Zhou P, Wu X and Yang D 2020 The role of O_2 in CdSeTe thin film deposition and CdSeTe/CdTe solar cell performance *Sol. Energy Mater. Sol. Cells* **214** 110595
[22] Kashuba A, Ilchuk H, Petrus R Y, Andriyevsky B, Semkiv I and Zmiyovska E 2022 Growth, crystal structure and theoretical studies of energy and optical properties of $CdTe_{1-x}Se_x$ thin films *Appl. Nanosci.* **12** 335–42
[23] Ablekim T, Duenow J N, Zheng X, Moutinho H, Moseley J, Perkins C L, Johnston S W, O'Keefe P, Colegrove E and Albin D S 2020 Thin-film solar cells with 19% efficiency by thermal evaporation of CdSe and CdTe *ACS Energy Lett.* **5** 892–6
[24] Çiriş A, Başol B M, Atasoy Y, Küçükömeroğlu T, Karaca A, Tomakin M and Bacaksız E 2021 Effect of CdS and CdSe pre-treatment on interdiffusion with CdTe in CdS/CdTe and CdSe/CdTe heterostructures *Mater. Sci. Semicond. Process.* **128** 105750
[25] Bai Z and Wang D 2012 Oxidation of CdTe thin film in air coated with and without a $CdCl_2$ layer *Phys. Status Solidi* a **209** 1982–7
[26] Zanio K 1978 *Cadmium Telluride* (Academic)
[27] Kumar S G and Rao K K 2014 Physics and chemistry of CdTe/CdS thin film heterojunction photovoltaic devices: fundamental and critical aspects *Energy Environ. Sci.* **7** 45–102
[28] Shah N A, Ali A, Ali Z, Maqsood A and Aqili A 2005 Properties of Te-rich cadmium telluride thin films fabricated by closed space sublimation technique *J. Cryst. Growth* **284** 477–85
[29] Khatun S, Banerjee A and Pal A J 2019 Nonlayered tellurene as an elemental 2D topological insulator: experimental evidence from scanning tunneling spectroscopy *Nanoscale* **11** 3591–8
[30] Abdul-Manaf N A, Salim H I, Madugu M L, Olusola O I and Dharmadasa I M 2015 Electro-plating and characterisation of CdTe thin films using $CdCl_2$ as the cadmium source *Energies* **8** 10883–903
[31] Wang G, Park M, Liu H-K, Wexler D and Chen J 2006 Synthesis and characterization of one-dimensional CdSe nanostructures *Appl. Phys. Lett.* **88** 193115
[32] Azhniuk Y M, Hutych Y I, Lopushansky V V, Raevskaya A E, Stroyuk A L, Kuchmiy S Y, Gomonnai A V and Zahn D R T 2007 Interplay of factors affecting Raman scattering in cadmium chalcogenide nanocrystals in dielectric media *J. Phys.: Conf. Ser.* **79** 012017
[33] Dharmadasa I M 2014 Review of the $CdCl_2$ treatment used in CdS/CdTe thin film solar cell development and new evidence towards *Improv. Understand. Coat.* **4** 282–307
[34] Fiducia T A, Mendis B G, Li K, Grovenor C R, Munshi A H, Barth K, Sampath W S, Wright L D, Abbas A and Bowers J W 2019 Understanding the role of selenium in defect passivation for highly efficient selenium-alloyed cadmium telluride solar cells *Nat. Energy* **4** 504–11
[35] Mahato S and Kar A 2015 Structural, optical and electrical properties of electrodeposited cadmium selenide thin films for applications in photodetector and photoelectrochemical cell *J. Electroanal. Chem.* **742** 23–29
[36] Kuciauskas D, Dippo P, Zhao Z, Cheng L, Kanevce A, Metzger W K and Gloeckler M 2015 Recombination analysis in cadmium telluride photovoltaic solar cells with photoluminescence spectroscopy *IEEE J. Photovolt.* **6** 313–8